IEEE Photonics Journal
An IEEE Photonics Society Publication

Open Access

Multichannel Transmission Through a Gold Strip Plasmonic Waveguide Embedded in Cytop

Volume 5, Number 3, June 2013

Behnam Banan
Mohammed Shafiqul Hai
Ewa Lisicka-Skrzek
Pierre Berini
Odile Liboiron-Ladouceur

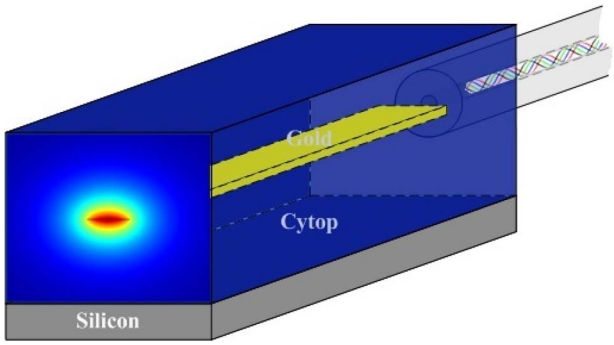

DOI: 10.1109/JPHOT.2013.2267537
1943-0655/$31.00 ©2013 IEEE

IEEE photonics SOCIETY

IEEE

Multichannel Transmission Through a Gold Strip Plasmonic Waveguide Embedded in Cytop

Behnam Banan,[1] Mohammed Shafiqul Hai,[1] Ewa Lisicka-Skrzek,[2] Pierre Berini,[2] and Odile Liboiron-Ladouceur[1]

[1]Department of Electrical and Computer Engineering, McGill University, Montreal, QC H3A0E9, Canada
[2]School of Electrical Engineering and Computer Science, and Department of Physics, University of Ottawa, Ottawa, ON K1N6N5, Canada

DOI: 10.1109/JPHOT.2013.2267537

Manuscript received May 20, 2013; accepted June 4, 2013. Date of publication June 10, 2013; date of current version June 19, 2013. Corresponding author: B. Banan (e-mail: behnam.banan@mail.mcgill.ca).

Abstract: In this paper, we experimentally characterize a low-loss polymer-based plasmonic waveguide and present its system-level performance for transmitting multiple on-off keying modulated channels (4×49 Gb/s). The same waveguide also exhibits the capability of transmitting multiple differential phase shift keying modulated channels (4×10 Gb/s). Signal transmission has been verified through bit-error-rate measurements. The plasmonic waveguide consists of a 3.6-mm-long, 5-μm-wide, and 35-nm-thick gold strip embedded in Cytop polymer and exhibits a total optical insertion loss of approximately 13 dB at a free-space optical wavelength of 1.55 μm.

Index Terms: Optical interconnects, long-range surface plasmon polaritons (SPPs), gold strip, low-loss polymer-based waveguide, Cytop, on-off keying (OOK), differential phase shift keying (DPSK).

1. Introduction

The demand for high bandwidth in high-performance computing and telecommunications equipment (routers) rises as the critical performance bottleneck shifts from processors to the interconnections. Considering the technological advances in processor technology, in the future, communication between processors or between cores in multicore processors requires high throughput links for distances in the range of millimeters. Additionally, 3-D-memory interfaces require interconnections with large capacity for distances from several millimeters to several centimeters [1]. At the system level, one prerequisite in the implementation of high-performance computing platforms is to have high-bandwidth, low-latency, and low-power interconnections. With minimum signal delay and power dissipation, photonics has been shown capable of carrying large amounts of information [2]. Integration of electronics and optics would resolve the issue of limited bandwidth caused by transmission loss, impedance mismatching, crosstalk, and electromagnetic interference [3]. In this regard, plasmonic structures [4]–[7] can potentially enable efficient and highly integrated optical interconnects for different applications (i.e., on-chip, off-chip, and chip-to-chip). The metal-dielectric structure of plasmonics provides a natural interface for guiding both light and electrical signals, which potentially leads to reduced energy consumption for optoelectronic

circuitry. There are a number of research works that support these unique capabilities of plasmonic structures through the demonstration of thermo-optic devices [8]–[11], where an electrical current is applied to the plasmonic waveguide in order to route the optical signal. There is also the demonstration of electronic and optical transmission lines [12], where the plasmonic waveguide can be used in both microwave and terahertz domains.

Surface plasmon polaritons (SPPs) are electromagnetic waves that propagate along an interface of two media with dielectric constants (ε) of opposite signs. Consequently, SPPs are confined by a dielectric-metal interface at optical frequencies (where $\mathrm{Re}\{\varepsilon_{\mathrm{metal}}\} < 0$ and $\mathrm{Re}\{\varepsilon_{\mathrm{dielectrics}}\} > 0$), having fields that decay exponentially into both media. For a structure comprised of a thin metal film of finite width, embedded in a homogeneous dielectric, corner modes and finite edge modes on the metal film couple to each other to form symmetric and asymmetric modes. The so-called long-range SPP (LRSPP) is a fundamental and symmetric mode, and its low attenuation leads to enhanced propagation length (up to several centimeters) at the expense of reduced confinement compared with the single-interface SPP [13]. Moreover, the structure has the potential to be used as both an optical and an electrical signal transmission line interconnecting elements that are separated by centimeters. These attributes and the ease with which the structures can be fabricated (particularly in polymer claddings) render them interesting for low-cost chip-to-chip interconnects between shared elements.

So far, a single-channel data transfer at 10 and 40 Gb/s through LRSPP waveguides implemented as gold strips embedded in ZPU450 polymer has been demonstrated with the lowest measured propagation loss of approximately 1.4 dB/cm for a gold strip with 14-nm thickness and 2-μm width [14]–[17]. ZPU450 polymer (supplied by ChemOptics, Inc. [18]) has a refractive index of about 1.45 at 1.55-μm wavelength, and it has been shown that the lower the refractive index of dielectric medium of a LRSPP waveguide, the lower the propagation loss [13], [14]. Signal transmission through dielectric-loaded SPP waveguides (DLSPPWs) with 12 channels at 40 Gb/s per channel has been demonstrated with high mode confinement [10]. However, DLSPPWs introduce large propagation loss limiting propagation lengths to hundreds of microns [19]. These features make the DLSPPWs promising for short-reach interconnections.

We have developed embedded thin gold strips in Cytop amorphous fluoropolymer. The main characteristics of Cytop for interconnect applications are its transparency, low refractive index, low dispersion coefficient, and good lamination properties [20]. The low refractive index of Cytop ($n = 1.3335$ at 1.55 μm) leads to lower LRSPP propagation loss compared with higher index materials such as ZPU450, but at the expense of lower confinement. For instance, theoretically, a gold strip 20-nm thickness and 5-μm width embedded in ZPU450 is expected to have approximately 6.5-dB/cm attenuation, and a mode field diameter (MFD) of approximately 8 μm laterally and 7 μm vertically [14]. On the other hand, the same gold strip fabricated in Cytop is expected to have approximately 3.6-dB/cm attenuation with lateral MFD of 8.2 μm and vertical MFD of 10.2 μm (see Section 2). Additionally, the low dispersion coefficient makes Cytop an interesting material as an optical signal transmission medium.

Previously, several passive LRSPP devices in Cytop have been characterized using an unmodulated signal [21]. We have also optically characterized 3.6-mm-long gold strips embedded in Cytop and demonstrated its capability to transmit single-channel data at 40 and 49 Gb/s with on-off keying (OOK) modulation [22]. In this paper, for the first time to the best of our knowledge, the capability of a strip plasmonic waveguide for multichannel data transmission is demonstrated by sending multiple optical OOK channels at 49 Gb/s. The investigation is extended to include transmission of multichannel optical signals modulated at 10 Gb/s using differential phase shift keying (DPSK) modulation format. The two modulation formats allow exploring the waveguide's transparency to either phase or amplitude modulation, which we believe is crucial to prove system-level performance of LRSPP waveguides in Cytop. Phase modulation is investigated as it is more sensitive to phase noise from possible nonlinear effects. In all measurements, the optical transmission is verified with bit-error-rate (BER) measurements.

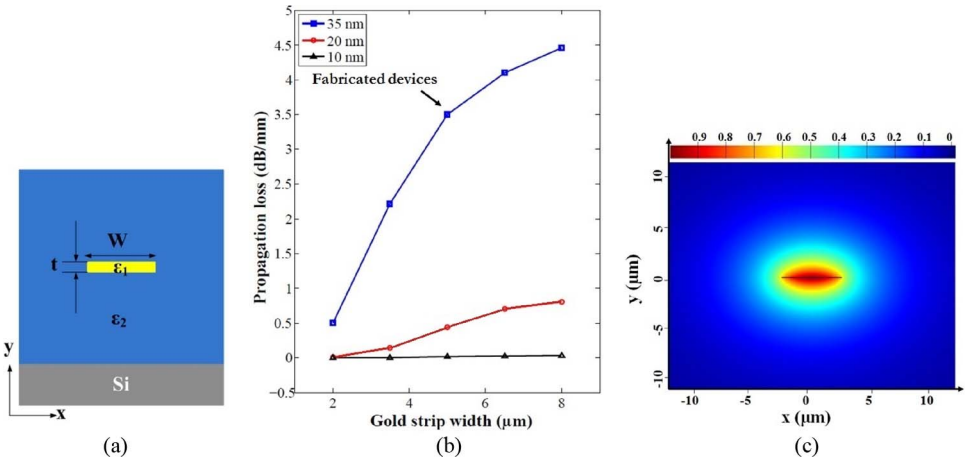

Fig. 1. (a) Schematic of the plasmonic strip waveguide cross section. (b) Simulated propagation loss as a function of gold strip width (w) and thickness (t). (c) The near-field image of the electric field $(\mathrm{Re}\{E_y\})$ distribution of the 5-μm-wide and 35-nm-thick gold strip. These dimensions were used for the fabricated devices.

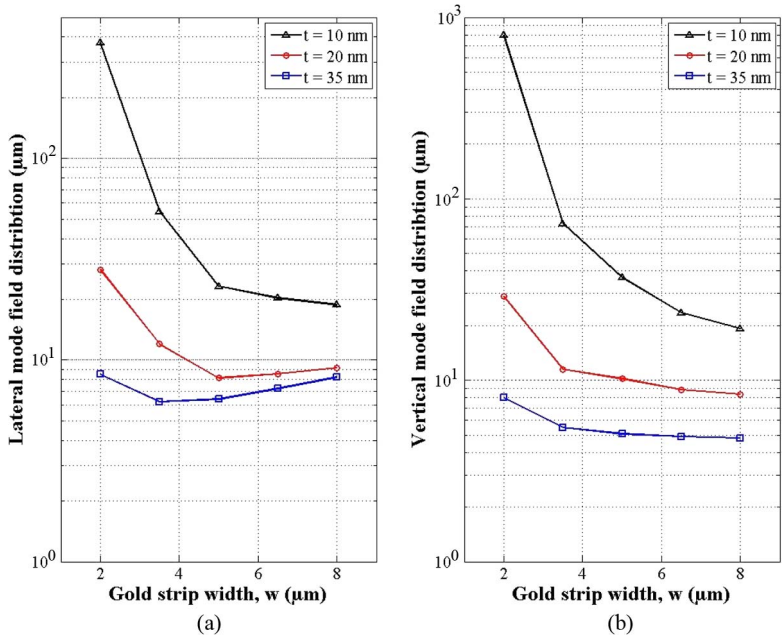

Fig. 2. Simulated (a) lateral and (b) vertical MFD as a function of gold strip width (w) and thickness (t).

2. Simulation

The schematic of the plasmonic strip waveguide is shown in Fig. 1(a). The relative permittivity ε_1 of the gold strip is assumed to be $-131.95 + 12.65i$ (refractive index, $n = 0.55 + 11.5i$) at a wavelength of 1.55 μm [23]. In simulation, thickness t is varied from 10 to 35 nm, and width w is varied from 2 to 8 μm in 1.5-μm increments. The dielectric is a Cytop amorphous fluoropolymer with a refractive index of 1.3335 at 1.55 μm [20] and is thick enough to accommodate LRSPP modes. Lumerical MODE Solutions software is used to obtain the propagation loss and the MFD. The software meshes the cross section of the waveguide using finite-difference algorithm and then solves Maxwell's equations by sparse matrix technique in order to find the effective index and the

mode profile. Fig. 1(b) illustrates the simulation results obtained for the propagation loss of different gold widths and thicknesses. As seen, the propagation loss decreases with decreasing thickness and width, as expected [13]. The lowest simulated propagation loss obtained for a 10-nm-thick gold film corresponds to 0.01902 dB/m. This is achieved when the width is designed to be 2 μm. Fig. 1(c) shows the near-field image of the electric field $(\mathrm{Re}\{E_y\})$ distribution of the 5-μm-wide and 35-nm-thick gold strip. These dimensions were used for the fabricated devices. In Fig. 2, the MFD along the lateral and vertical slices through the center of the waveguide of the LRSPP mode is shown. The MFD in this case is defined as the full-width mode electric field E_y spot size at the $1/e$ points. In general, both lateral and vertical MFDs become larger with decreasing gold thickness and width. The exception is the lateral MFD for 10- and 20-nm-thick gold strips with a width in the range of 8 down to 5 μm, and this is attributed to the fact that the lateral MFD is always larger than the width of the metal strip [24]. Hence, there is a clear tradeoff between the propagation loss [see Fig. 1(b)] and the MFD (see Fig. 2). These results are in good agreement with reported work by others [14]–[17].

3. Fabrication

The structure used in the experimental demonstration was fabricated as follows. First, a 7-μm-thick layer of the Cytop polymer is coated on a silicon wafer using multiple spin coating and solvent evaporation to form the lower cladding. The wafer is then patterned using bilayer reentrant photolithography. A 35-nm-thick layer of gold (Au) is then deposited using E-beam evaporation followed by wet solvent stripping to reveal the metal structures. The structures are then covered by an additional 7-μm-thick layer of Cytop to form the upper cladding. Gold strip dimensions were chosen to provide a reasonable tradeoff between attenuation and mode confinement. In addition, based on computations, at the chosen dimensions, the coupling loss between the LRSPP waveguide and a standard single-mode fiber (SMF-28, MFD of 10.4 μm and NA of 0.14) is sufficiently low (0.52 dB/facet). Moreover, there are some fabrication challenges, which need to be considered while determining the gold strip thickness. Finally, the wafer is diced into several dies, and the length of the LRSPP waveguides is set to 3.6 mm (fabrication details can be found in [25]).

4. Measurements

4.1. Single NRZ-OOK Channel at 40 and 49 Gb/s

Fig. 3(a) shows the schematic of the experimental setup for insertion loss and mode profile measurements. The input power at 1.55 μm (10 dBm) is provided by a laser source with its fiber-coupled output passing through a polarization controller. The polarized output signal (9.5 dBm) is sent through a Mach–Zehnder modulator (MZM), which has a 3-dB electrical bandwidth of 33 GHz (The electrical amplifier of the MZM has a 3-dB bandwidth of 40 GHz). The dc bias of the MZM is set at 1.8 V (approximately $V_\pi/2$) to produce an OOK signal with maximum eye opening. A 50-Gb/s 4:1 MUX clocked by a signal generator drives the modulator at 40 and 49 Gb/s with a $2^{31}-1$ pseudorandom binary sequence (PRBS) non-return-to-zero (NRZ) electrical data using a pulse pattern generator (PPG). Then, the signal is amplified to an optical power level of 10 dBm using an erbium-doped fiber amplifier (EDFA). The modulated optical signal passes through a polarization controller exciting LRSPPs with TM polarized light. Fig. 3(b) shows one of the fabricated waveguides with the electrical dc pads attached to it, which are designed to investigate the thermo-optic effect of the LRSPP mode (not used in this paper). The output signal is edge coupled to the chip through a 10-μm single-mode fiber with alignment control accomplished using a 6-axis nanopositioner stage. Then, the output power from the structure is collected using a 20$\times$ microscope objective and collimated. The beam passes through a variable aperture (500 μm to 18 mm) and then is divided by a 50/50 nonpolarizing cubic beam splitter to simultaneously direct the light to the IR-camera and the power meter. Fig. 3(c) illustrates the far-field captured LRSPP when the aperture is open (aperture diameter of 18 mm). The background light is primarily attributed to the random polarization of the amplified spontaneous emission (ASE) noise emerging from the EDFA and leaking of the uncoupled light through the polymer. Fig. 3(d) shows the far-field captured

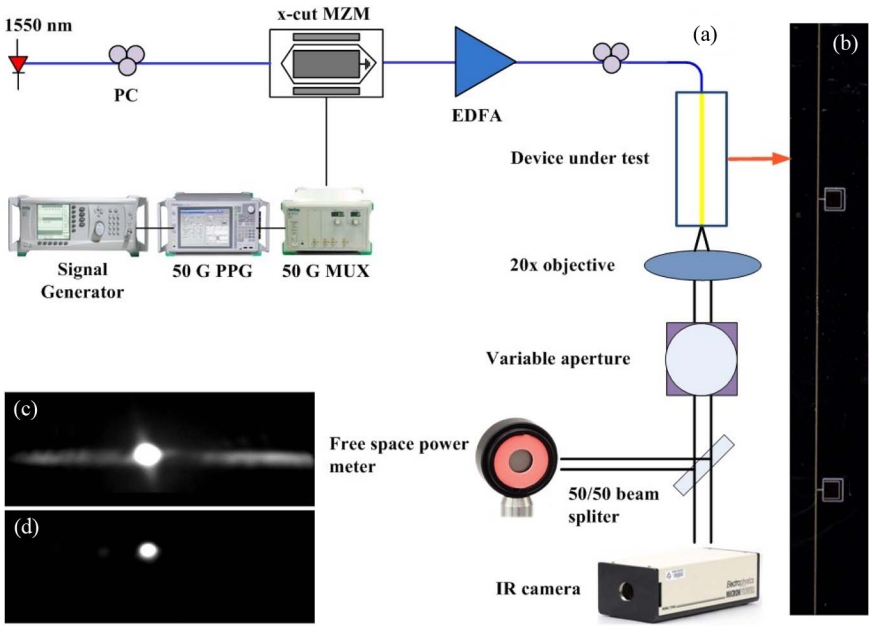

Fig. 3. (a) Schematic of the setup to measure the insertion loss and capture the mode profile. (b) Fabricated devices. (c) Far-field captured LRSPP and scattered light from the cladding layer (open aperture). (d) Far-field captured LRSPP (partially closed aperture and attenuated).

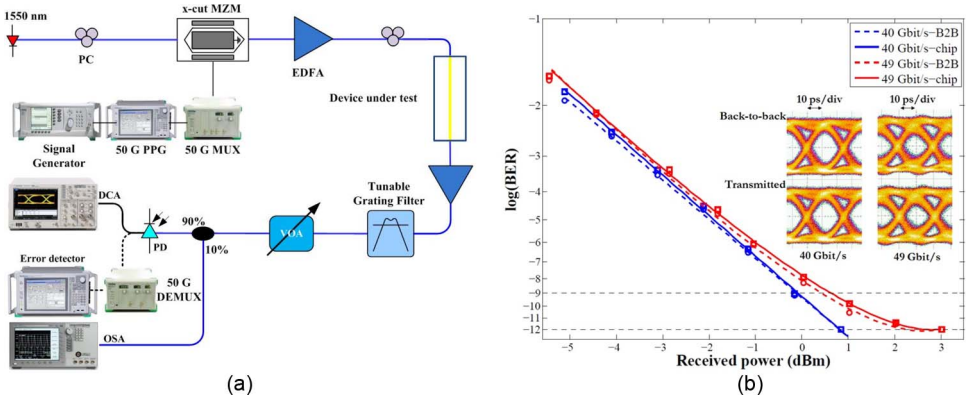

Fig. 4. (a) Schematic of the setup for single channel at 1550 nm to measure the BER. (b) Measured BER with respect to the received power for single channel at 40 and 49 Gb/s. The inset shows the eye diagrams.

LRSPP when the aperture is partially closed in order to block the background light and also attenuated by approximately 50% using a free-space attenuator. The average measured insertion loss from seven different straight waveguides with 3.6 mm in length is 13.2 dB, which is in good agreement with the simulation result. Simulation predicted 3.45-dB/mm attenuation, which corresponds to 12.42-dB propagation loss for the length of 3.6 mm. In addition, the expected coupling loss between the fabricated LRSPP waveguide and SMF-28 is 0.52 dB/facet. Therefore, considering the insertion loss measurement setup [see Fig. 3(a)], the expected total loss was 12.94 dB, which is close to the measured values.

The experimental setup for the eye diagram and BER measurements is illustrated in Fig. 4(a). The input to the chip is similar to the previous setup. At the output, the power is collected using a 10-μm single-mode fiber, and alignment control is accomplished by a 3-axis nano-positioner stage.

Then, the signal is amplified using a second EDFA and passes through a tunable filter (0.85 nm) to remove out-of-band ASE noise. The output is connected to a variable optical attenuator (VOA), and then, a 10/90 coupler is used to send the signal to an optical spectrum analyzer (OSA) and a photodetector (3-dB bandwidth of 47 GHz), respectively. The signal is analyzed using a digital communication analyzer with 30 GHz of RF bandwidth and a 50-Gb/s 1:4 DEMUX connected to a 50-Gb/s capable error detector.

Fig. 4(b) shows the measured BER for a single channel with respect to the received power at the photodetector for the back-to-back and transmitted signals. In the case of back-to-back measurements, the device is replaced by an attenuator set to the corresponding plasmonic waveguide total loss (approximately 14 dB). The inset shows the eye diagrams for the back-to-back (top) and transmitted signals (bottom) at 40 and 49 Gb/s, respectively. As seen from the measurements, the LRSPP waveguide effectively transmits optical data with negligible power penalties at 40 and 49 Gb/s, and error-free performance $(\text{BER} < 10^{-9})$ has been achieved. The power penalty between the two data rates is 0.86 dB at BER of 10^{-9}. The noise floor for 49 Gb/s transmission is caused by the bandwidth limitation of the optoelectronic components used in the experimental setup, which primarily originates from the MZM's optimum point of operation being at 40 Gb/s.

4.2. Multiple NRZ-OOK Channel at 49 Gb/s

Fig. 5(a) shows the schematic of the experimental setup for four channels with OOK modulation transmission. Four 10-dBm distributed feedback laser sources are each fiber coupled to polarization controllers and are emitting at 1536.12, 1536.93, 1537.71, and 1538.59 nm. The four channels are separated by approximately 0.79 nm matching the 100-GHz ITU grid. The polarized output signal (9.5 dBm) from each channel is sent to a 4×1 coupler and then passes through the modulator. A 50-Gb/s 4:1 MUX clocked by a signal generator drives the modulator at 49 Gb/s with a $2^{31} - 1$ PRBS electrical data using a PPG. Then, the signal is amplified to a power level of 7.5 dBm per channel using an EDFA. Finally, the modulated optical signals passes through a polarization controller to obtain LRSPPs from TM polarized light.

Fig. 5(b) shows the optical spectrum of the four channels at the input and output of the chip (with 0.06-nm resolution) corresponding to points A and B in Fig. 5(a), respectively. The input signal is edge coupled to the fabricated chip through a 10-μm single-mode fiber using a 6−axis nano-positioner stage. At the output, the power is collected using a 10-μm single-mode fiber aligned with a 3-axis nano-positioner stage. Then, the signal is amplified to 7 dBm per channel using a second EDFA and then passes through a tunable filter (0.4 nm) to select the channel under test and remove out-of-band ASE noise. The signal is again amplified with an EDFA, and the output is connected to a VOA, and a 10/90 coupler is used to simultaneously send the signal to an OSA and a photodetector. Fig. 6(a) shows the measured BER with respect to the received power at the photodetector for the back-to-back and transmitted signals. In the case of back-to-back measurements, the device is replaced by an attenuator set to the corresponding plasmonic waveguide total loss (approximately 15 dB). The 1-dB increase in total loss compared with single-channel transmission is due to the wavelength dependency of the LRSSP propagation loss. Error-free performance is achieved only for two channels, and a noise floor appears, which we believe is due to the additional ASE noise associated with the third EDFA. This leads to an OSNR limitation of the experimental setup. Fig. 6(b) shows the eye diagrams for the back-to-back (top) and transmitted signals (bottom) at 49 Gb/s. As observed, the eye diagrams are noisier compared with that of the single-channel transmission. However, both the back-to-back and transmitted eye diagrams exhibit the same level of noise. Thus, the power penalty is relatively low. At a BER of 10^{-7}, where the noise floor is minimum, the power penalty is negligible, except for the channel at 1536.93 nm where it is less than 1 dB.

4.3. Multiple NRZ-DPSK Channel at 10 Gb/s

Fig. 7(a) shows the schematic of the experimental setup for four channels with the DPSK modulated signal transmission. The setup is similar to the OOK transmission setup described in the

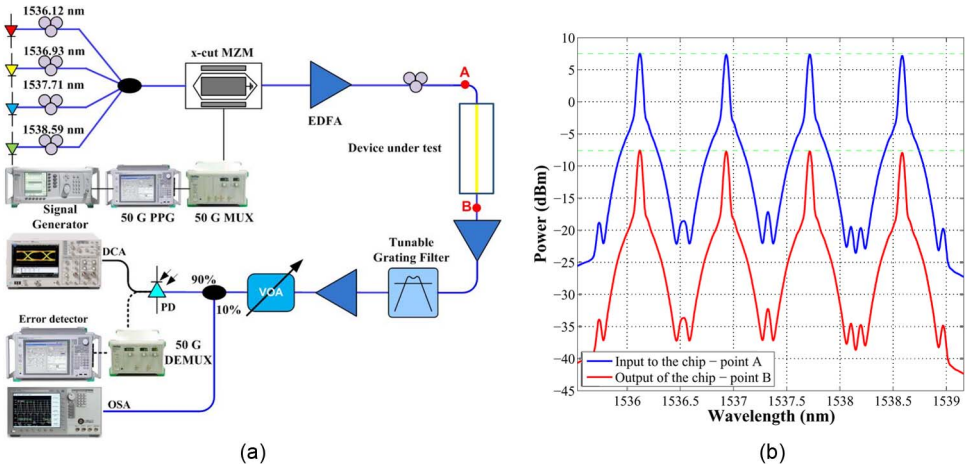

Fig. 5. (a) Schematic of the setup for four channels OOK signals transmission to measure the BER. (b) Input (blue) and output (red) signals of the chip with OOK modulation at 49 Gb/s corresponding to points A and B shown in (a), respectively.

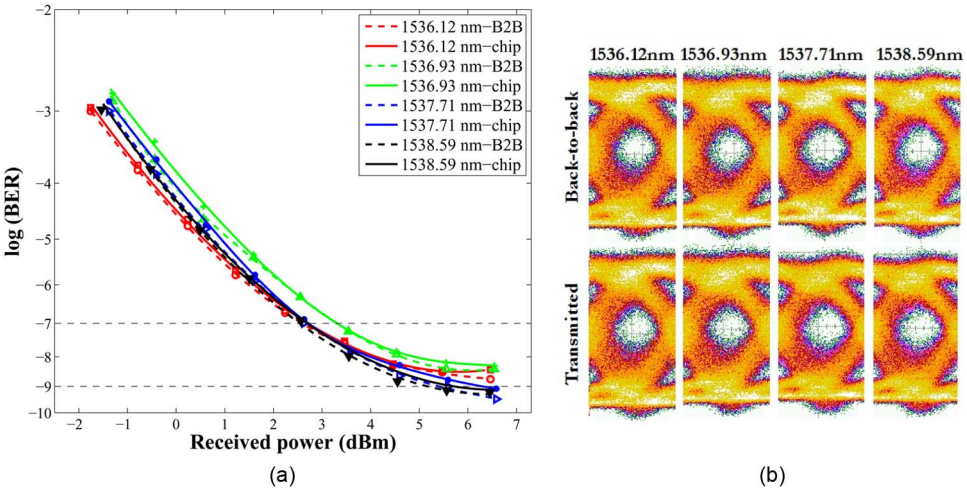

Fig. 6. (a) Measured BER and (b) eye diagrams for the back-to-back and transmitted signals for four channels with OOK modulation at 49 Gb/s.

previous section, except at the input where the MZM has a 3-dB electrical bandwidth of 12 GHz (The maximum input data rate to the electrical amplifier of the MZM is 12.5 Gb/s). The dc bias of the MZM is set at 2.5 V (approximately V_π) to generate the DPSK modulated signal with maximum eye opening. A 50-Gb/s 4:1 MUX clocked by a signal generator drives the modulator at 10 Gb/s with a $2^{31} - 1$ PRBS electrical data using a PPG. Additionally, at the receiver end, a 10 Gb/s DPSK delay line demodulator is added, which converts the phase variation of the DPSK modulated signal to intensity variation. Another EDFA is added after the demodulator to compensate for the insertion loss of the demodulator. Fig. 7(b) shows the optical spectrum of the four channels at the input and output of the chip, corresponding to points A and B in Fig. 7(a), respectively. Fig. 8 shows the measured BER with respect to the received power at the photodetector for the back-to-back and transmitted DPSK signals. From Fig. 8, it is seen that error-free operation $(\text{BER} < 10^{-9})$ is achieved for all channels with negligible power penalty for two channels and less than 1 dB for the other two channels. Furthermore, roughly a 1-dB wavelength dependency is observed, and this can be attributed to the frequency response of the delay line demodulator. The insets show the received

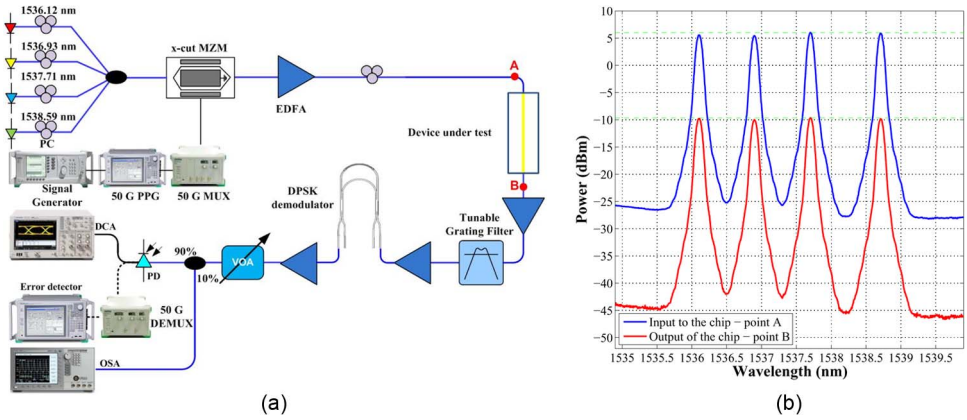

Fig. 7. (a) Schematic of the setup for four channels DPSK signals transmission to measure the BER. (b) Input (blue) and output (red) signals of the chip with DPSK modulation at 10 Gb/s corresponding to points A and B shown in (a), respectively.

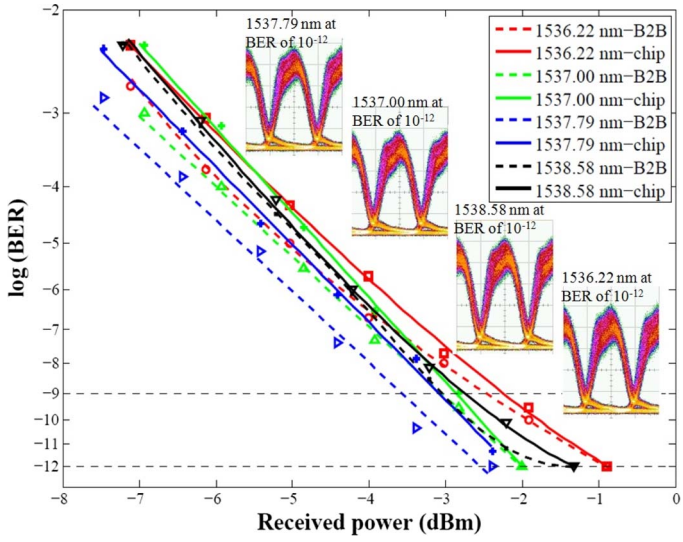

Fig. 8. Measured BER for four channels with DPSK modulation at 10 Gb/s. The insets show eye diagrams of the transmitted signal for all channels at BER of 10^{-12}.

open eye diagrams produced from single-ended DPSK demodulation for transmitted signals through the chip for all channels at BER of 10^{-12}. For received eye diagrams, the constructive output port of the DPSK demodulator is shown for the two channels. The DPSK eye diagrams show the presence of noise in the system, which is attributed to the ASE noise emerging from four EDFAs in the experimental setup. Furthermore, our measurements showed no sign of phase shift due to possible nonlinear effects in the waveguide.

5. Discussion

The need for low-cost and power-efficient on-chip and off-chip optical interconnects is increasing, and plasmonic structures supporting long-range modes are good candidates for these applications. Therefore, demonstration of system-level performance of passive LRSPP waveguides is essential in order to prove their capability of being implemented as optical interconnects and to examine their advantages and disadvantages.

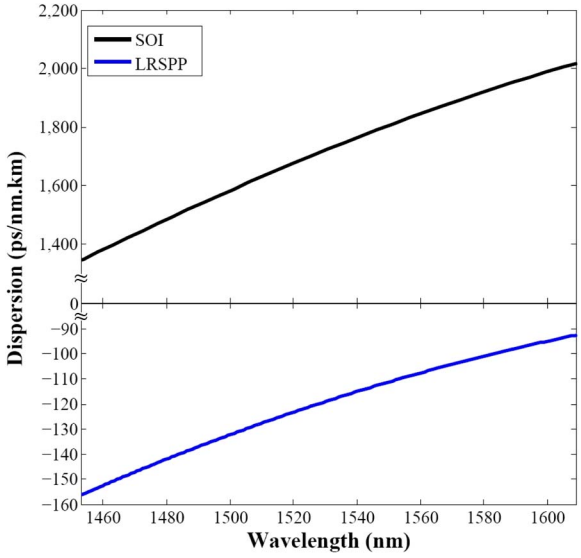

Fig. 9. Calculated dispersion for SOI waveguide with 525-nm width and 226-nm thickness and embedded gold strip with 5-μm width and 35-nm thickness in Cytop polymer.

In this paper, the fabricated gold strips (thickness of 35 nm and width of 5 μm) showed an average insertion loss of 13.2 dB at 1.55 μm (measurements) with lateral MFD of 6.5 μm and vertical MFD of 5 μm (simulation, Fig. 2). The propagation loss of 35-nm-thick gold strip can be reduced by a factor of 7 with decreasing its width down to 2 μm, and yet maintain reasonable optical mode confinement (lateral and vertical MFD of 8.5 μm). Thus, even more efficient LRSPP waveguide embedded in Cytop is achievable.

The effective transmission of multichannel high data rate signals with either OOK or DPSK modulation format through LRSPP waveguides is confirmed by means of BER measurements and eye diagrams. Results suggest no degradation due to the possible dispersion, nonlinearities, and wave vector mismatch. Based on the transmission measurements compared with the back-to-back measurements, the LRSPP waveguide introduces negligible dispersion. This is in good agreement with expectations as Cytop has very low material dispersion at 1.55 μm [26], and the waveguides are short with low confinement (i.e., the fields do not overlap strongly with the dispersive metal). Fig. 9 shows the calculated dispersion parameter of the LRSPP mode as a function of wavelength. The waveguide exhibits about $D = -111$ ps$/$(nm $\cdot$ km) at 1.55 μm. This is low compared with silicon-on-insulator (SOI) waveguides, which are proposed for on-chip photonic interconnections. For silicon waveguides of 525-nm width and 226-nm thickness, the dispersion parameter $D \simeq 1800$ ps$/$(nm $\cdot$ km) (see Fig. 9) and ~ 4400ps$/$(nm $\cdot$ km) (experimental [27]).

The dispersion length can be estimated for a half-pulsewidth at the $1/e$ power points, $T_0 = 5$ ps (for a 50-Gb/s data rate), using the following equation [27], i.e.,

$$L_D = \frac{2\pi c_0 T_0^2}{\lambda^2 D} \tag{1}$$

where c_0 is the speed of light, λ is the wavelength, and D is the dispersion parameter. It is found that the theoretical dispersion length of our LRSPP waveguide is around 177 m at 50 Gb/s, which is 16 times longer than that of the mentioned SOI waveguide (approximately 11 m). Therefore, considering its length (3.6 mm), dispersion is negligible, and the structure is considered bandwidth unlimited. In this paper, the bandwidth limitation is attributed to the optoelectronics used in the experimental setup.

The nonlinearity that may distort the signal originates from the nonlinear electron oscillation at the metal-dielectric interface caused by the incident photons, leading to second- and third-order

nonlinear processes [28], [29]. Furthermore, in the case of LRSPP excitation, a misalignment between the incident wave and the propagating plasmonic mode leads to a reduction in coupling efficiency. These impairments were negligible in our demonstration. Taking into account all these factors, one may draw a conclusion that the LRSPP waveguide is capable of transmitting much higher bit-rates (50 Gb/s and more) per channel, as well as larger aggregated bandwidth.

6. Conclusion

In this paper, we have demonstrated that plasmonic strip waveguides are capable of transmitting NRZ-OOK data signals at 4×49 Gb/s, as well as NRZ-DPSK data signals at 4×10 Gb/s. Potentially higher data rates are achievable as the dispersion length of the fabricated waveguides is estimated at 177 m for 50-Gb/s data. The 3.6-mm-long gold strip with a thickness of 35 nm and a width of 5 μm in Cytop supports a LRSPP mode with 13.2 dB of insertion loss at 1.55 μm. Our results suggest that plasmonic strip waveguides are capable of being implemented as short-reach broadband optical interconnects.

References

[1] Y. Arakawa, T. Nakamura, Y. Urino, and T. Fujita, "Silicon photonics for next generation system integration platform," *IEEE Commun. Mag.*, vol. 51, no. 3, pp. 72–77, Mar. 2013.

[2] M. A. Taubenblatt, "Optical interconnects for high performance computing," *J. Lightwave Technol.*, vol. 30, no. 4, pp. 448–458, Feb. 2012.

[3] Y. Takagi, A. Suzuki, T. Horio, T. Ohno, T. Kojima, T. Takada, S. Iio, K. Obayashi, and M. Okuyama, "Low-loss chip-to-chip optical interconnection using multichip optoelectronic package with 40 Gb/s optical I/O for computer applications," *J. Lightwave Technol.*, vol. 28, no. 20, pp. 2956–2963, Oct. 2010.

[4] H. A. Atwater, "The promise of plasmonics," *Sci. Amer.*, vol. 296, no. 4, pp. 56–62, Apr. 2007.

[5] M. L. Brongersma and V. M. Shalaev, "The case for plasmonics," *Science*, vol. 328, no. 5977, pp. 440–441, Apr. 2010.

[6] W. L. Barnes, A. Dereux, and T. W. Ebbesen, "Surface plasmon subwavelength optics," *Nature*, vol. 424, no. 6950, pp. 824–830, Aug. 2003.

[7] J. J. Ju, S. Park, M. S. Kim, J. T. Kim, S. K. Park, J. M. Lee, J. S. Choe, and M. H. Lee, "Data transfer for optical interconnectors using long range-SPP transmission lines," presented at the Proc. OFC/NFOEC Tech. Dig., Los Angeles, CA, 2012, OW3E.66192159.

[8] K. Hassan, J. C. Weeber, L. Markey, A. Dereux, A. Pitilakis, O. Tsilipakos, and E. E. Kriezis, "Thermo-optic plasmo-photonic mode interference switches based on dielectric loaded waveguides," *Appl. Phys. Lett.*, vol. 99, no. 24, p. 241110, Dec. 2011.

[9] G. Giannoulis, D. Kalavrouziotis, D. Apostolopoulos, S. Papaioannou, A. Kumar, S. I. Bozhevolnyi, L. Markey, K. Hassan, J. C. Weeber, A. Dereux, M. Baus, M. Karl, T. Tekin, O. Tsilipakos, A. K. Pitilakis, E. E. Kriezis, K. Vyrsokinos, H. Avramopoulos, and N. Pleros, "Data transmission and thermo-optic tuning performance of dielectric-loaded plasmonic structures hetero-integrated on a silicon chip," *IEEE Photon. Technol. Lett.*, vol. 24, no. 5, pp. 374–376, Mar. 2012.

[10] D. Kalavrouziotis, S. Papaioannou, G. Giannoulis, D. Apostolopoulos, K. Hassan, L. Markey, J. C. Weeber, A. Dereux, A. Kumar, S. I. Bozhevolnyi, M. Baus, M. Karl, T. Tekin, O. Tsilipakos, A. Pitilakis, E. E. Kriezis, H. Avramopoulos, K. Vyrsokinos, and N. Pleros, "0.48Tb/s ($12\times$ 40 Gbit/s) WDM transmission and high-quality thermo-optic switching in dielectric loaded plasmonics," *Opt. Express*, vol. 20, no. 7, pp. 7655–7662, Mar. 2012.

[11] G. Gagnon, N. Lahoud, G. A. Mattiussi, and P. Berini, "Thermally activated variable attenuation of long-range surface plasmon-polariton waves," *J. Lightwave Technol.*, vol. 24, no. 11, pp. 4391–4402, Nov. 2006.

[12] B. Banan, A. Salehiomran, and O. Liboiron-Ladouceur, "Investigation of a flexible on-chip interconnection using a plasmonic strip waveguide," in *Proc. IEEE Photon. Conf.*, 2011, pp. 13–14.

[13] P. Berini, "Plasmon-polariton waves guided by thin lossy metal films of finite width: Bound modes of symmetric structures," *Phys. Rev. B, Condens. Matter*, vol. 61, no. 15, pp. 10484–10503, Apr. 2000.

[14] J. J. Ju, S. Park, M. S. Kim, J. T. Kim, S. K. Park, Y. J. Park, and M. H. Lee, "Polymer-based long-range surface plasmon polariton waveguides for 10 Gbit/s optical signal transmission applications," *J. Lightwave Technol.*, vol. 26, no. 11, pp. 1510–1518, Jun. 2008.

[15] S. Park, M. S. Kim, J. T. Kima, S. K. Park, J. J. Jua, and M. H. Lee, "Long range surface plasmon polariton waveguides at 1.31 and 1.55μm wavelengths," *Opt. Commun*, vol. 281, no. 8, pp. 2057–2061, Apr. 2008.

[16] J. T. Kim, S. Park, J. J. Ju, S. K. Park, M. S. Kim, and M. H. Lee, "Low-loss polymer-based long-range surface plasmon waveguide," *IEEE Photon. Technol. Lett.*, vol. 19, no. 18, pp. 1374–1376, Sep. 2007.

[17] J. J. Ju, S. Park, M. S. Kim, J. T. Kim, S. K. Park, Y. J. Park, and M. H. Lee, "40 Gbit/s light signal transmission in long-range surface plasmon waveguide," *Appl. Phys. Lett.*, vol. 91, no. 17, p. 171117, Oct. 2007.

[18] ChemOptics, Inc., Daejeon, Korea. [Online]. Available: http://www.chemoptics.co.kr

[19] V. S. Volkov, Z. Han, M. G. Nielsen, K. Leosson, H. Keshmiri, J. Gosciniak, O. Albrektsen, and S. I. Bozhevolnyi, "Long-range dielectric-loaded surface plasmon polariton waveguides," *Opt. Lett.*, vol. 36, no. 21, pp. 4278–4280, Nov. 2011.

[20] Asahi Glass Company, Wilmington, DE, USA, Technical Information Cytop, distributed by Bellex International Corporation. [Online]. Available: http://www.bellexinternational.com

[21] H. Fan, R. Buckley, and P. Berini, "Passive long-range surface plasmon-polariton devices in Cytop," *Appl. Opt.*, vol. 51, no. 10, pp. 1459–1467, Apr. 2012.
[22] B. Banan, M. S. Hai, E. Lisicka-Shzek, P. Berini, and O. Liboiron-Ladouceur, "49 Gbit/s optical transmission through long-range surface plasmon polariton waveguide," in *Proc. IEEE IPC*, 2012, pp. 278–279.
[23] R. Charbonneau, C. Scales, I. Breukelaar, S. Fafard, N. Lahoud, G. Mattiussi, and P. Berini, "Passive integrated optics elements based on long-range surface plasmon polaritons," *J. Lightwave Technol.*, vol. 24, no. 1, pp. 477–494, Jan. 2006.
[24] I. Breukelaar, R. Charbonneau, and P. Berini, "Long-range surface plasmon-polariton mode cutoff and radiation in embedded strip waveguides," *J. Appl. Phys.*, vol. 100, no. 4, p. 043104, Aug. 2006.
[25] C. Chiu, E. Lisicka-Skrzek, R. N. Tait, and P. Berini, "Fabrication of surface plasmon waveguides and devices in Cytop with integrated microfluidic channels," *J. Vac. Sci. Technol. B*, vol. 28, no. 4, pp. 729–735, Jul. 2010.
[26] Y. Koike and M. Asai, "The future of plastic optical fiber," *NPG Asia Mater.*, vol. 1, no. 1, pp. 22–28, Oct. 2009.
[27] E. Dulkeith, F. Xia, L. Schares, J. Green, and Y. A. Vlasov, "Group index and group velocity dispersion in silicon-on-insulator photonic wires," *Opt. Express*, vol. 14, no. 9, pp. 3853–3863, May 2006.
[28] Y. R. Shen, "Surface properties probed by second-harmonic and sum-frequency generation," *Nature*, vol. 337, no. 6207, pp. 519–525, Feb. 1989.
[29] S. Palomba and L. Novotny, "Nonlinear excitation of surface plasmon polaritons by four-wave mixing," *Phys. Rev. Lett.*, vol. 101, pp. 056802-1–056802-3, Aug. 2008.